Journal of Coordination Chemistry

Synthesis, antimicrobial screening, and DNA-binding/cleavage of new pyrazole-based binuclear Co^{II}, Ni^{II}, Cu^{II}, and Zn^{II} complexes

Naveen V. Kulkarni [a] & Vidyanand K. Revankar [a]

[a] Department of Studies in Chemistry , Karnatak University , Pavate Nagar, Dharwad 580 003, Karnataka, India
Published online: 18 Feb 2011.

PLEASE SCROLL DOWN FOR ARTICLE

Taylor & Francis
Taylor & Francis Group

Synthesis, antimicrobial screening, and DNA-binding/cleavage of new pyrazole-based binuclear Co^{II}, Ni^{II}, Cu^{II}, and Zn^{II} complexes

NAVEEN V. KULKARNI and VIDYANAND K. REVANKAR*

Department of Studies in Chemistry, Karnatak University, Pavate Nagar,
Dharwad 580 003, Karnataka, India

Pyrazolato endogenous bridged binuclear Co^{II}, Ni^{II}, Cu^{II}, and Zn^{II} complexes were prepared and characterized by spectro-analytical methods. The hexadentate N$_4$S$_2$ donor was synthesized by condensation of 3,5-dichloroformyl-1H-pyrazole with thiosemicarbazide in dry ethanol. All the complexes were binuclear and octahedral in nature. The ligand and complexes are screened for antimicrobial and DNA-binding/cleavage activities. The binding/cleavage activities with *Escherichia coli* DNA are monitored with absorption, hydrodynamic, thermal denaturation, and electrophoresis studies. The ligand possesses significant activity against microbes which is further enhanced upon complexation. The DNA-binding study reveals classical intercalation. The Ni^{II} and Cu^{II} complexes exhibit higher binding ability.

Keywords: Pyrazole; Thiosemicarbazide; Antimicrobial activity; DNA-binding study; Intercalation

1. Introduction

Pyrazole derivatives possess versatile coordination toward transition metal ions and wide applications, such as anticancer, antifungal [1], and antibacterial activities [2]. Deprotonated pyrazole can be a diazine bridge, exploited for its potential binucleating ability [3, 4]. Nucleophilicity and steric accessibility of pyrazole nitrogens can be altered by appropriate ring substitutions [3–6]. In this study, biologically active thiosemicarbazide is incorporated to the pyrazole core as a side-chelating arm expected to enhance the ligational suppleness and pharmacological applications. The ligand interacts with transition metal ions and the compounds are screened for antimicrobial activity. A large body of evidence indicates that complexes exhibit biological activity by binding to DNA and inhibiting replication. Coordination complexes can directly change the 3-D structure of DNA with interaction of the N-7 nitrogen of the nucleotide. DNA-binding/cleavage ability of a compound depends on the nucleophilicity and lability of the ligand and nature of the metal ion. Complexes that have been studied for DNA-binding abilities are usually coordinatively saturated, inert to substitution, rigid, and cannot

---

*Corresponding author. Email: vkrevankar@rediffmail.com

N.V. Kulkarni and V.K. Revankar

directly coordinate to DNA, but typically bind to DNA by non-covalent interactions, such as electrostatic, intercalative, and groove binding. In addition, metal complexes often induce DNA strand scission by a number of mechanistic pathways, thus marking their binding sites. Hence, interest in synthetic biomimetic anticancer agents with active metal centers can directly interact with the DNA of infected cells. Complexes can be used as structural probes and diagnostic tools in cancer treatment [7]. Considering the inhibitory action of pyrazole-based metal complexes toward the growth of microorganisms, DNA-binding/cleaving ability of the compounds is investigated by interaction with *Escherichia coli* DNA by monitoring with absorption, hydrodynamic, thermal denaturation, and electrophoresis studies.

Several other complexes were prepared and studied for their DNA binding [8–12] but the utility of pyrazole-bridged binuclear complexes in this regard is still unattempted. Therefore in this article we report the synthesis, characterization, and DNA binding/ cleavage of pyrazole-bridged binuclear complexes.

2. Materials and methods

2.1. *Analysis and physical measurements*

Elemental analysis was carried out on a Thermo Quest elemental analyzer; metal estimation was done by standard procedures [13] and the results are presented in table 1. Molar conductivity measurements in DMF were made on an ELICO-CM-82 conductivity bridge with cell having cell constant of $0.51 \, \text{cm}^{-1}$. Magnetic susceptibility measurements were made at room temperature using a Faraday balance with $Hg[Co(SCN)_4]$ as a calibrant. ^1H-NMR spectra were recorded in DMSO-d_6 on a Bruker-300 MHz spectrometer at room temperature using TMS as internal reference. IR spectra were recorded in a KBr matrix using an Impact-410 Nicolet (USA) FT-IR spectrometer $(4000–400 \, \text{cm}^{-1})$. The ESR spectrum of the copper complex was carried out on a Varian E-4X-band EPR spectrometer using TCNE as the g-marker. TG and DTA measurements of the complexes were recorded in nitrogen on a Universal V2 4F TA instrument at heating rate of $10°\text{C} \, \text{min}^{-1}$ from $25–800°\text{C}$. FAB mass spectra were

Table 1. Elemental analyses and conductivities of compounds.

Compound	Elemental analysis (%) Calculated (Found)						Molar conductivity $(\Omega^{-1}\text{cm}^2\text{mol}^{-1})$
	C	H	N	M	S	Cl	
LH_3	27.72 (28.01)	3.63 (3.78)	36.96 (37.12)	–	21.12 (21.24)	–	–
$[Co_2LH_2(\mu Cl)Cl_2(H_2O)_2]$	14.79 (15.02)	2.29 (2.46)	19.73 (20.02)	20.76 (21.03)	11.24 (10.68)	18.76 (18.00)	13.4
$[Ni_2LH_2(\mu Cl)Cl_2(H_2O)_2]$	14.81 (14.57)	2.29 (2.18)	19.75 (20.13)	20.61 (20.83)	11.28 (11.84)	18.78 (18.64)	18.2
$[Cu_2(LH_2)_2]Cl_2 \cdot 2H_2O$	20.19 (20.58)	2.41 (2.12)	26.92 (26.84)	15.26 (16.02)	15.38 (15.84)	8.53 (8.31)	184.3
$[Zn_2LH_2(\mu Cl)Cl_2(H_2O)_2]$	14.46 (14.63)	2.23 (2.35)	19.29 (18.94)	22.52 (22.73)	11.02 (10.53)	18.34 (18.21)	16.2

drawn from a JEOL SX 102/DA-6000 mass spectrometer using Argon/Xenon (6 kV, 10 mA) as the FAB gas and 3-nitrobenzylalcohol as matrix. Cyclic voltammetric studies were performed at room temperature in DMF with oxygen-free condition created by purging pure nitrogen gas with a CHI1110A Electrochemical analyzer (USA) comprising a three-electrode assembly of glassy carbon working electrode, platinum auxiliary electrode, and non-aqueous Ag^+/AgCl reference electrode. Tetramethylammoniumchloride (0.01 M) was used as a supporting electrolyte and the instrument was standardized by ferrocene/ferrocenium redox couple. Electronic spectra of the complexes were recorded on a Hitachi 150-20 spectrophotometer with scan range of 1000–200 nm. The same instrument, equipped with a temperature controlling thermostat, is used for DNA-binding studies (absorption and thermal denaturation). Bio-Rad Trans illuminator and a Polaroid camera were used in the gel electrophoresis experiment and an Oswald micro-viscometer is used for hydrodynamic measurements.

2.2. *Preparation of LH₃ (1H-pyrazole-3,5-dicarboxy bis(thiosemicarbazide))*

Commercially obtained 1H-pyrazole-3,5-dicarboxylic acid (0.156 g, 0.01 M) was refluxed with thionylchloride (10 mL) in anhydrous condition for 4 h at 110–120°C. The content was then evaporated to dryness to remove excess thionylchloride, giving a pasty mass which was allowed to cool. A solution of thiosemicarbazide (0.184 g, 0.02 M) in dry ethanol was added dropwise and refluxed for 3 h. Resulting solution was cooled in an ice bath to get a colorless amorphous solid, which was separated by filtration, dried over anhydrous $CaCl_2$, and recrystallized from ethanol (the reaction pathway is represented in figure 1).

2.3. *Preparation of complexes*

Metal(II) chloride {$CoCl_2 \cdot 6H_2O$ (0.475 g, 0.02 M), $NiCl_2 \cdot 6H_2O$ (0.474 g, 0.02 M), $CuCl_2 \cdot 2H_2O$ (0.341 g, 0.002 M) and $ZnCl_2$ (0.271 g, 0.02 M)} in methanol (100 mL) was added with stirring to a methanolic solution of LH_3 (0.318 g, 0.01 M) and refluxed on a water bath for 3–4 h. Obtained solid complex was separated by filtration, washed with hot ethanol and dried *in vacuo* (proposed structures of complexes in figure 2).

2.4. *Antibiogram analysis of compounds against bacteria*

The medium used in the analysis was prepared by adding 10 g of peptone and 10 g of sodium chloride to homogeneous mixture of 5 g of yeast extract and 20 g of nutrient
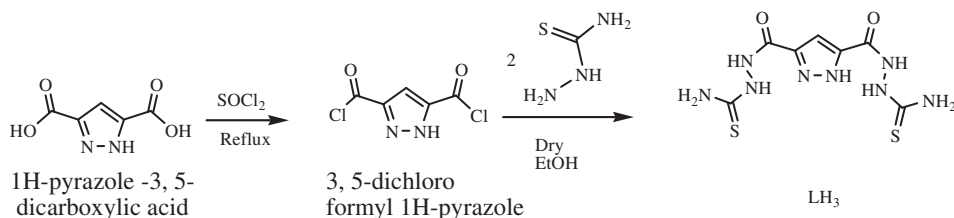

1H-pyrazole -3, 5-
dicarboxylic acid

3, 5-dichloro
formyl 1H-pyrazole

LH₃

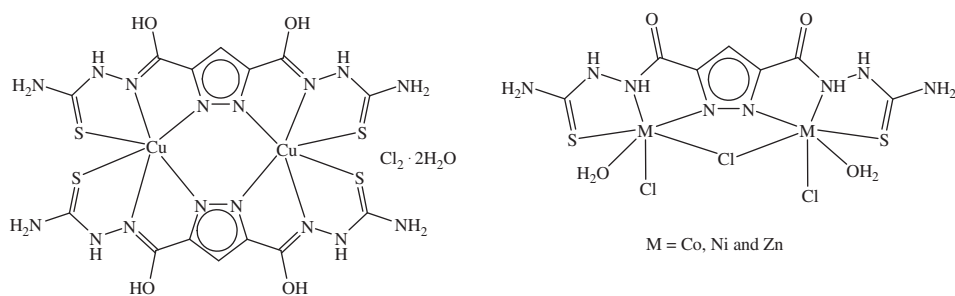Figure 1.   Scheme representing the preparation of LH_3.

Figure 2.   Proposed structures of the complexes.

agar taken in 1000 mL of distilled water. Initially, stock cultures of *E. coli* and *Pseudomonas aeruginosa* were revived by inoculating in broth media and grown at 37°C for 18 h. Agar plates of the above media were prepared and wells were made in the plate. Each plate was inoculated with 150 μL of 18 h old cultures and spread evenly on the plate. After 20 min, the wells were filled with 100 μL of each compound (10 mg mL^{-1} in DMF). Control plates with gentamycin (10 mg mL^{-1}) and DMF were also prepared. All plates were incubated at 37°C for 24 h and the diameter of inhibition zone noted in centimeters. The values were compared with that of gentamycin and DMF. Samples showing significant inhibition were selected for further determination of minimum inhibition concentration (MIC). The MICs of compounds were determined by assaying at 500 and 250 μg concentrations along with standard gentamycin with same concentration. Cultures were grown for 24 h and the zones were compared with that of gentamycin and percentage of inhibition calculated.

2.5.   *Antibiogram analysis of compounds against fungi*

Potato dextrose agar medium used in the analysis was prepared by mixing 20 g of dextrose to the filtrate obtained by 250 g of peeled potato boiled for 20 min, squeezed, and filtered; the volume was made up to 1000 mL by adding distilled water. Initially, stock cultures of *Aspergillus niger* and *Cladosporium* were revived by inoculating in broth media and grown at 37°C for 48 h. The agar plates of the above media were prepared and wells were made in the plates. Each plate was inoculated with 150 μL of 48 h old cultures and spread evenly on the plate. After 20 min, the wells were filled with 500 μL of each compound (10 mg mL^{-1} in DMF). The control plates with fluconazole (10 mg mL^{-1}) and DMF were also prepared. All the plates were incubated at 37°C for 48 h and the diameter of inhibition zone noted in centimeters. The values were compared with that of fluconazole and DMF. The samples showing significant inhibition were selected for further determination of MIC. The MICs were determined by assaying at 500 and 250 μg concentrations along with standard fluconazole at the same concentrations. The cultures were grown for 48 h and the zones were compared with that of fluconazole and the percentage of inhibition calculated.

2.6. *DNA-binding studies*

2.6.1. Isolation of DNA *E. coli.* Nutrient broth peptone $(10\,g\,L^{-1})$, yeast extract $(5\,g\,L^{-1})$, and NaCl $(10\,g\,L^{-1})$ were used for culturing of *E. coli*. The 50 mL medium was prepared, autoclaved for 15 min at 121°C, 15 lb pressure. Autoclaved media were inoculated with the seed culture and incubated at 37°C for 24 h for *E. coli*. The fresh bacterial culture (1.5 mL) was centrifuged to obtain the pellet and dissolved in 0.5 mL of lysis buffer (100 mmol L^{-1} *tris* pH 8.0, 50 mmol L^{-1} EDTA, and 10% SDS) to which 0.5 mL of saturated phenol was added and incubated at 55°C for 10 min. The incubated solution was centrifuged at 10,000 rpm for 10 min and to the supernatant an equal volume of chloroform, isoamyl alcohol (24 : 1), and 1/20th volume of 3 mol L^{-1} sodium acetate (pH 4.8) were added. The mixture was again centrifuged at 10,000 rpm for 10 min and to the supernatant three volumes of chilled absolute alcohol was added. The precipitated DNA was separated by centrifugation, dried, dissolved in TE buffer (10 mmol L^{-1} *tris* pH 8.0, 1 mmol L^{-1} EDTA), and stored cool.

The concentration of DNA per nucleotide [C (p)] was measured using its known extinction coefficient at 260 nm $(\sim6600\,(\text{mol}\,L^{-1})^{-1}cm^{-1})$. The absorbance at 260 nm (A260) and at 280 nm (A280) for DNA was measured to check its purity. The ratio A260/A280 was 1.88, indicating that DNA was satisfactorily free from protein. *Tris* buffer [5 mmol L^{-1} *tris* (hydroxymethyl) aminomethane, *tris*, pH 7.2, 50 mmol L^{-1} NaCl] was used for absorption, viscosity, and thermal denaturation experiments.

2.6.2. Absorption studies. The complexes were dissolved in DMSO and then diluted to the desired concentration with water. Spectroscopic titrations were carried out by adding increasing amounts of DNA to a solution of the complex at a fixed concentration contained in a quartz cell. The UV-Vis spectra were recorded after equilibration at 20°C for 10 min after each addition. The intrinsic binding constant K_b was determined from the plot of $A_0/[A - A_0]$ *versus* $[\text{DNA}]^{-1}$ according to the equation

$$A_0/[A - A_0] = \varepsilon_G/[\varepsilon_{H-G} - \varepsilon_G] + \varepsilon_G/[\varepsilon_{H-G} - \varepsilon_G] \times 1/K\,[\text{DNA}],$$

where A_0 and A are the absorbance in the free complex and absorbance at given DNA concentration, respectively. [DNA] is the concentration of DNA in base pairs, and ε_G and ε_{H-G} are the apparent absorption coefficients in free and DNA bound form of complex, respectively. The data were fitted to the above equation and a graph was obtained with a slope equal to $\varepsilon_G/[\varepsilon_{H-G} - \varepsilon_G] \times 1/K$ and an intercept equal to $\varepsilon_G/[\varepsilon_{H-G} - \varepsilon_G]$. Hence K_b was obtained from the ratio of the intercept to the slope [14].

2.6.3. Hydrodynamic measurements (viscosity measurements). The measurements were carried out using an Oswald micro-viscometer maintained at constant temperature (23°C) in a thermostat bath. The DNA concentration was kept constant in all samples (100 μM), but the complex concentration was increased each time (from 20 to 80 μM). Mixing of the solution was achieved by bubbling nitrogen through the viscometer. The flow time was measured with a digital stopwatch. Sample flow times were measured three times and the mean value was used. Data are presented in a plot of $(\eta/\eta_0)^{1/3}$ *versus* the ratio [complex]/[DNA], where η and η_0 are the specific viscosity of DNA in the

presence and absence of the complex, respectively. The values of η and η_0 were calculated using the equation:

$$\eta = (t - t_0)/t_0,$$

where t is the observed flow time of DNA containing solution and t_0 is the flow time of DNA solution alone. Relative viscosities for DNA were calculated from the relation (η/η_0) [15].

2.6.4. Thermal denaturation.   Thermal denaturation studies were carried out on a UV-spectrometer equipped with temperature controlling thermostat. The melting curves (T_m-curve) of both free *E. coli* DNA and DNA-bound complexes were obtained by measuring the hyperchromicity of DNA at 260 nm as a function of temperature. The melting temperatures were measured with 60 μM DNA in phosphate buffer at pH 6.8 ($\mu = 0.2$ mol L^{-1}M NaCl). The temperature was scanned from 25°C to 85°C at a rate of 5°C min^{-1}. The melting temperature (T_m) was taken as the mid-point of the hyperchromic transition.

2.6.5. Electrophoresis.   For gel electrophoresis experiments [14], solutions of complexes in DMF (1 mg mL^{-1}) were prepared and these test samples (1 μg) were added to the genomic DNA samples of *E. coli* and incubated for 2 h at 37°C. Agarose gel was prepared in TAE buffer (4.84 g *tris* base, pH 8.0, 0.5 mol L^{-1}EDTA L^{-1}. pH 7.3), the solidified gel attained at ~55°C was placed in an electrophoresis chamber flooded with TAE buffer. After that 20 μL of each incubated complex-DNA mixture (mixed with bromophenol blue dye at 1 : 1 ratio) was loaded on the gel along with standard DNA marker and electrophoresis was carried out under a TAE buffer system at 50 V for 2 h. At the end of electrophoresis, the gel was carefully stained with ethidium bromide (EB) solution (10 μg mL^{-1}) for 10–15 min and visualized under UV light using a Bio-Rad Trans illuminator. The illuminated gel was photographed using a Polaroid camera (a red filter and Polaroid film were used).

3. Results and discussion

3.1. *Chemistry*

3.1.1. Molar conductivity measurements.   Molar conductance values of all the complexes at room temperature in DMF with 10^{-3} mol dm^{-3} fall in the range 13.4–18.2 Ω^{-1} cm^2 mol^{-1}, which indicates non-electrolytic complexes (table 1). The copper complex exhibits 1 : 2 electrolytic nature by the high molar conductance value (184.3 Ω^{-1}cm^2 mol^{-1}) [16].

3.1.2. Infrared spectral analysis.   IR spectral details are presented in table 2. The ligand shows sharp absorptions around 3300 and 3200 cm^{-1} attributed to –NH$_2$ and –NH. A very strong band at 1645 cm^{-1} is assigned to amidic carbonyl stretch and band at 1532 cm^{-1} is assigned to pyrazole ring ν(C=N). The thione (C=S) form of ligand is

Table 2. IR spectral data (in cm^{-1}).

Compound	ν(−OH) Water	ν(−OH) Imidol	ν(NH$_2$)	ν(NH)	ν(NH) Pyrazole	ν(C=O) Amide	ν(C=N) Pyrazole	ν(N−N)	ν(C=S) Thioamide		ν(M−N)
LH$_3$	–	–	3371 b	3263 m	3178 s	1644 s	1532 s	1000 m	1286 m	803 s	–
[Co$_2$LH$_2$(μCl)Cl$_2$(H$_2$O)$_2$]	3449 b	-	3300 b	3257m	–	1645 m	1565 s	977 s	1216s	766 s	477 s
[Ni$_2$LH$_2$(μCl)Cl$_2$(H$_2$O)$_2$]	3430 b	-	3286 b	3257m	–	1645 m	1566 s	977 s	1214 m	767 s	490 s
[Cu$_2$(LH$_2$)$_2$]Cl$_2$·2H$_2$O	3450 b	3400 s	3341 b	3260 m	–	–	1568 m	1018 m	1226 m	768 s	462 s
[Zn$_2$LH$_2$(μCl)Cl$_2$(H$_2$O)$_2$]	3454 b	–	3320 b	3255 m	–	1641 m	1562 s	982 m	1231 m	765 s	471 s

s, sharp; m, medium; and b, broad.

suggested by the thioamidic absorptions observed at 1286 and 803 cm^{-1} [17]. For Cu^{II} complex disappearance of ν(C=O) and appearance of a new band at 1630 cm^{-1}, which may be assigned to ν(C=N), suggest imidol formation and coordination through azomethine nitrogen [18]. Appearance of a sharp peak at 3400 cm^{-1} attributable to ν(–OH) supports this. The unaltered sharp peak observed at 1645 cm^{-1} in all other complexes indicates coordination of amidic carbonyl. Coordination of hydrazine NH was suggested in these complexes due to the change in ν(N–N). In all complexes, pyrazole ring nitrogens are involved in ligation as diazine bridge, suggested by the blue shift in the stretching frequency of ring C=N and a sharp non-ligand band observed at 460 cm^{-1} attributable to ν(M–N). Thioamidic bands that have major contribution from C=S decrease in intensity with shift to low frequency, indicating thioketo mode of coordination [17, 19].

3.1.3. ^{1}H-NMR spectral studies. ^{1}H-NMR of the ligand and its Zn^{II} complex were carried out from 0 to 16 ppm. The ligand displays a sharp singlet at 9.88 ppm, attributable to N–H of pyrazole [20]; disappearance in the complex reveals formation of pyrazolide ion and coordination of pyrazole as an endogenous bridge. In the ligand, primary amine and amide protons resonate at 7.60 and 9.01 ppm, respectively, and peaks around 7.67 and 7.90 ppm were assigned for thioamidic and pyrazole ring protons. Upon complexation amide protons shift down field suggesting nitrogen coordination and the other protons experience a small shift due to the changed electronic environment from chelation. Appearance of a broad peak at 3.40 ppm reveals the presence of coordinated water.

3.1.4. UV-Vis spectral studies.   Electronic spectra were recorded in DMF from 200 to 1000 nm. Ligand exhibits a band around 270 nm due to intraligand $\pi \to \pi^*$ transition, which is unaltered in spectra of complexes. Absorbance at 350 nm is assigned for $n \to \pi^*$ transition of the imine and transitions around 275–300 are due to $n \to \pi^*$ transition of carbonyl [21]. In the cobalt complex, the band at 371 nm is assigned to LMCT transition (absorption coefficient, $\varepsilon \sim$30,000 lcm^{-1} mol^{-1}). Bands at 460 and 674 nm ($\varepsilon \sim$150 lcm^{-1} mol^{-1}) are attributed to d $\to$ d transitions, ^{4}T$_{1g} \to {}^4$A$_{2g}$ and ^{4}T$_{1g}$(F) $\to {}^4$T$_{1g}$(P) for octahedral structure. Octahedral Co^{II} complexes usually show three bands, in this case, the first band due to ^{4}T$_{1g}$(F) $\to {}^4$T$_{2g}$ occurs in the near infrared region and is not observed. In Ni^{II} complex, the lowest energy band at 910 nm ($\varepsilon \sim$100 lcm^{-1} mol^{-1}) was due to ^{3}A$_{2g} \to {}^3$T$_{2g}$(ν_1) and bands at 612 ($\varepsilon \sim$150 lcm^{-1} mol^{-1}) and 440 nm ($\varepsilon \sim$200 lcm^{-1} mol^{-1}) were assigned to ^{3}A$_{2g} \to {}^3$T$_{1g}$(ν_2), and ^{3}A$_{2g} \to {}^3$T$_{1g}$(P)(ν_3), respectively. These three spin-allowed d-d bands indicate octahedral Ni complex [20]. The copper complex exhibits a band around 600 nm with a low ε value ($\varepsilon \sim$100 lcm^{-1} mol^{-1}), absent in the zinc complex, assigned to d $\to$ d transition. The intense band observed at 420 nm is assigned for ligand to metal charge transfer. The electronic spectrum of the zinc complex shows bands at 270–300 ($\varepsilon \sim$15,000 lcm^{-1} mol^{-1}) and 350–400 nm ($\varepsilon \sim$25,000 lcm^{-1} mol^{-1}), accounting for intraligand and LMCT transitions, respectively.

3.1.5. Magnetic properties.   The copper complex exhibits effective magnetic moment, μ_{eff}, of 1.68 BM at 303 K. The low value suggests existence of an endogenous pyrazole

bridge with possible spin–spin interaction [5]. The room temperature magnetic moments of *bis*-complexes of nickel and cobalt complexes were 2.76 and 4.32 BM, respectively, suggesting distorted octahedral geometry [22, 23], which is well-supported by spectral data.

3.1.6. EPR spectral study. The X-band EPR spectrum of Cu^{II} complex in a solid form in the region of 9000 MHz with corresponding field intensity of $\sim$3000 Gauss exhibits isotropic intense broad signal of $g_{iso} = 2.038$ with no hyperfine splitting. This type of EPR spectrum was assigned for complexes having large organic ligand substituents. The broadening in signal may be attributed to existence of dipolar interaction in the complex. Further broadening suggests similar chemical environment for both copper ions [3, 18].

3.1.7. FAB mass spectral studies. FAB mass spectral studies support the proposed structures of the complexes (figure 2). FAB mass spectrum of copper complex shows molecular ion peak at m/z 832, suggesting dimeric structure for the complex with ligand to metal ratio 2:2. The mass spectrum of nickel complex shows highest mass peak at m/z 567, suggesting complex with ligand to metal ratio 1:2. Cobalt and zinc complexes are the same as nickel, supported by analytical and spectral analysis.

3.1.8. Thermal studies. Thermal stability and decomposition pattern of the complexes were analyzed by TG and DTA studies. TG analysis of the complexes has been carried out in nitrogen with a heating rate of $10°C\,min^{-1}$. Decomposition of Cu^{II} complex takes place in three stages: the first step corresponds to mass loss of 4.32% at 50–140°C attributed to loss of two water molecules. The corresponding DTA at 117°C signifies an endothermic process. The second stage of mass loss of 8.52% at 117–220°C with DTA peak at 193°C represents exothermic process corresponding to liberation of two chlorides as HCl. The weight loss of 14.5% at 240–340°C indicates decomposition of ligand (DTA peak at 336°C, endothermic). The final decomposition product was metal oxide. For the Ni complex, weight loss of 5.4% at 50–140°C with exothermic DTA peak at 135°C indicates loss of two coordinated water molecules. The liberation of two chlorides as HCl corresponds to about 15.27% of weight loss at 134–420°C with endothermic DTA peak at 385°C. Decomposition was concluded with formation of stable metal oxide. TG–DTA studies of Co^{II} and Zn^{II} complexes show similar decomposition pattern as Ni^{II} complex.

3.1.9. Cyclic voltammetric studies. Cyclic voltammetric study of ligand and complexes in DMSO (0.001 M) was carried out from -1.0 to 1.0 V in O_2-free conditions with different scan rates (0.05, 0.1 and $0.15\,V\,s^{-1}$) (table 3). Analysis reveals that only the copper complex exhibits (figure S1 in Supplementary material) redox properties with the ligand and other complexes electrochemically innocent in the applied potential range. An anodic peak in the voltammogram of the copper complex at $E_{pa} = 0.50$–0.53 V represents oxidation, $Cu^{II} \rightarrow Cu^{III}$. During the reverse scan, i.e. cathodic potential scan, two peaks are observed, attributed to the $Cu^{III} \rightarrow Cu^{II}$ and $Cu^{II} \rightarrow Cu^{I}$ reduction with peak potentials at $E_{pc1} = 0.32$–0.36 V and $E_{pc2} = 0.08$–0.12 V. The high value of ΔE_p, separation between the cathodic and anodic peak potentials ($E_{pa} - E_{pc}$)

Table 3. Cyclic voltammetric results.

Complex	Scan rate ($V\,s^{-1}$)	E_{pa} (V)	E_{pc} (V)		ΔE_p (V)[a]	$E_{1/2}$ (V)[a]	I_{pc}/I_{pa}
[Cu$_2$(LH$_2$)$_2$]Cl$_2$ · 2H$_2$O	0.15	0.53	0.32	0.08	0.21	0.42	1.22
	0.1	0.51	0.34	0.1	0.17	0.42	1.20
	0.05	0.50	0.36	0.12	0.14	0.43	1.18

[a]($\Delta E_p = E_{pa} - E_{pc}$; $E_{1/2} = [E_{pc} + E_{pa}]/2$).

greater than 60 mV, indicates quasi-reversible redox process [24]. The electrochemical activity of copper complex and its quasi-reversible nature can be explained in terms of flexibility and size of the coordination cavity and the size of the metal ions in the different oxidation states. Further detailed studies are required to understand the chemical reactions following the electron transfers which are helpful in enzyme catalysis.

3.2. Biochemistry

3.2.1. Bioactivity of the compounds against fungi and bacteria. In order to study comparative biological activities, the ligand and its complexes were screened for antibacterial and antifungal activities against bacteria *E. coli*, *P. aeruginosa* and fungi *A. niger*, *Cladosporium* at 500 and 250 μg concentrations in DMF; the latter is treated as an MIC. The activities are compared with gentamycin for bacteria and fluconazole for fungi, and the results are tabulated in tables 4 and 5. The ligand is less active against fungus *Cladosporium*, bacteria *P. aeruginosa* and moderately active against bacteria *E. coli* and fungus *A. niger*. An enhancement in activity is observed upon complexation. The copper complex shows moderate activity against *E. coli* and *P. aeruginosa* bacteria at 500 and 250 μg concentration and extremely high activity (as good as the internal standard) against fungus *A. niger* at both concentrations, and against *Cladosporium* it shows moderate inhibitory activity. The nickel complex shows moderate activity at 500 μg and low inhibition at MIC level against *E. coli* and *P. aeruginosa* bacteria. It is moderately active against *A. niger* and *Cladosporium*. The cobalt and zinc complexes exhibit slight antifungal and antibacterial activities at both concentrations. Enhancement in antimicrobial properties from complexation is often related to increased lipophilicity and inertness of certain metal–ligand linkages, which protects the molecule against enzymatic degradation. The activity is expected to be reinforced by combined effect of the ligand and metal [25].

3.2.2. DNA-binding/cleavage studies

3.2.2.1. *Absorption studies.* The binding of complexes and drugs to the DNA helix has been characterized through absorption spectral titrations by following the changes in absorbance and shift in the wavelength as a function of added concentration of DNA (50–200 μM) with ligand and its metal complexes (500 μM) *E. coli* DNA, in different concentrations.

Table 4. Analysis of antibacterial activity.

Compound	500 µg				250 µg			
	E. coli		P. aeruginosa		E. coli		P. aeruginosa	
	Zone of inhibition in cm[a]	Percentage of inhibition	Zone of inhibition in cm[a]	Percentage of inhibition	Zone of inhibition in cm[a]	Percentage of inhibition	Zone of inhibition in cm[a]	Percentage of inhibition
Gentamycin	3.2	100	2.9	100	3.0	100	2.4	100
Ligand	0.9	28	0.5	17	0.5	17	0	0
$[Co_2LH_2(\mu Cl)Cl_2(H_2O)_2]$	0.9	28	0.6	21	0.6	20	0.2	7
$[Ni_2LH_2(\mu Cl)Cl_2(H_2O)_2]$	1.3	40	1	34	0.8	27	0.4	17
$[Cu_2(LH_2)_2]Cl_2 \cdot 2H_2O$	1.8	56	1.3	45	1	33	0.5	17
$[Zn_2LH_2(\mu Cl)Cl_2(H_2O)_2]$	1	31	0.8	28	0.6	20	0.3	12
DMF	0.1	3	–	–	–	–	–	–

[a]Measurements involve ± 0.01 error limit.

Table 5.   Analysis of the antifungal activity.

|	500 μg				250 μg			
	A. niger		Cladosporium		A. niger		Cladosporium	
Compound	Zone of inhibition in cm[a]	Percentage of inhibition	Zone of inhibition in cm[a]	Percentage of inhibition	Zone of inhibition in cm[a]	Percentage of inhibition	Zone of inhibition in cm[a]	Percentage of inhibition
Fluconazole	1.2	100	0.9	100	1.1	100	0.8	100
Ligand	0.4	33	0.2	22	–	–	–	–
[Co$_2$LH$_2$(μCl)Cl$_2$(H$_2$O)$_2$]	0.5	42	0.3	33	0.1	9	0.1	12
[Ni$_2$LH$_2$(μCl)Cl$_2$(H$_2$O)$_2$]	0.8	67	0.4	44	0.4	36	0.3	37
[Cu$_2$(LH$_2$)$_2$]Cl$_2$ · 2H$_2$O	1.3	108	0.5	56	0.9	82	0.4	50
[Zn$_2$LH$_2$(μCl)Cl$_2$(H$_2$O)$_2$]	0.6	50	0.3	33	0.2	18	0.1	12
DMF	–	–	–	–	–	–	–	–

[a]Measurements involve ± 0.01 error limit.
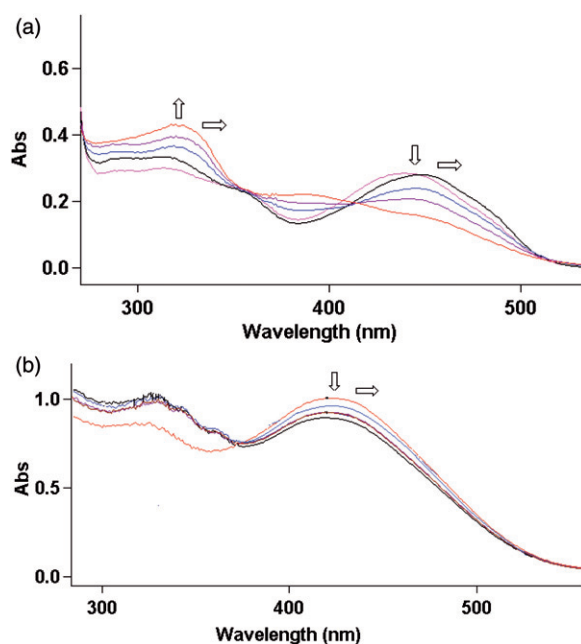
Figure 3. Absorption spectrum showing the variation of absorption with increase in DNA concentration for: (a) [Ni$_2$LH$_2$(μCl)Cl$_2$(H$_2$O)$_2$] and (b) [Cu$_2$(LH$_2$)$_2$]Cl$_2 \cdot$ 2H$_2$O.

For nickel complex (figure 3a), the broad band at 440 nm and intraligand transition at 310 nm were monitored as a function of added DNA. Increase in amount of DNA decreases molar absorptivity (hypochromism) as well as red shift of $\sim$8–10 nm (hypsochromic shift) for the band at 440 nm and increases molar absorptivity (hyperchromism) with 8–10 nm of hypsochromic shift (red shift) for the band at 310 nm, indicating intercalative interaction of complex with DNA. Isosbestic point at 406 nm confirms the binding of complex with DNA. The intrinsic binding constant K_b determined by a plot of $A_0/[A-A_0]$ *versus* [DNA]$^{-1}$, 1.6×10^4 M^{-1}, is moderate compared with classical intercalators ($K_b \sim 10^6$) suggesting moderate intercalative interaction. The copper complex shows hypochromism with a bathochromic shift of 3–5 nm for the band at 420 nm, assigned for LMCT of complex upon addition of increasing amount of DNA, indicating intercalative binding mode (figure 3b). The binding constant, $K_b = 1.5 \times 10^4$ M^{-1}, suggests moderate interaction between DNA and the complex. The ligand, cobalt, and zinc complexes show low hypochromism as well as an insignificant shift in wavelength of the monitored bands with increase in added DNA concentration, suggesting low binding capacity of ligand and complexes toward DNA. The intrinsic binding constants calculated, 2.1×10^3, 4.5×10^3 and 6.6×10^3 M^{-1}, respectively, for ligand, cobalt, and zinc complexes suggest mild intercalative interaction with DNA [26].

3.2.2.2. *Viscometric measurements.* Hydrodynamic methods such as viscometric measurements in which solution viscosity of DNA is sensitive to changes in effective length of DNA is a critical test for inferring the binding mode (intercalation or other
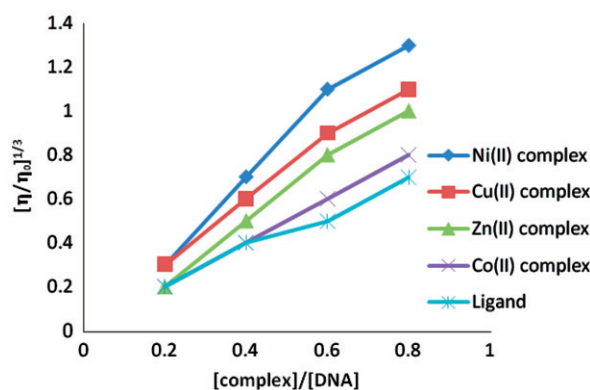
Figure 4. Effect of increasing concentration of compound on viscosity of DNA at 23°C.

binding modes) of DNA in solution. Intercalation of drugs like EB causes a significant increase in viscosity of DNA solutions due to increase in separation of base pairs at intercalation sites and hence an increase in overall DNA contour length. On the other hand, molecules that bind exclusively in DNA grooves typically cause less pronounced (positive or negative) or no changes in the DNA solution viscosity. Viscosity measurements were carried out on solution of *E. coli* DNA (100 µM) by varying the concentration of added compounds (20–80 µM) under appropriate conditions. Values of $(\eta/\eta_0)^{1/3}$, where η and η_0 are the specific viscosity of DNA in the presence and absence of complex, were plotted against [compound]/[DNA] (figure 4). The results reveal that all complexes and ligand bound to *E. coli* DNA show increase in relative viscosities with an increase in the [compound]/[DNA] ratio suggesting the intercalative binding mode of the compounds with DNA [15], consistent with results obtained from absorption studies. Change in viscosity caused by the nickel and copper complexes were more significant than others, indicating strong intercalation of the complexes.

3.2.2.3. *Thermal denaturation studies.* Thermal behaviors of DNA in the presence of complexes can give insight to their conformational changes when temperature is raised, offering information about the interaction strength of complexes with DNA. When temperature of solution increases, the double-stranded DNA gradually dissociates to single strands and generates a hyperchromic effect on absorption spectra of DNA bases ($\lambda_{\max} = 260$ nm). In order to identify this transition process, the melting temperature (T_m), defined as the temperature where half of the total base pairs are unbound, is introduced. According to the literature, the interaction of natural or synthesized intercalators generally results in considerable increase in T_m. Hence the DNA melting experiment is useful in establishing the extent of intercalation binding between compound and DNA. The T_m of *E. coli* DNA in the absence of added complex was found to be 58 ± 1°C in our experimental conditions. Under the same conditions, the presence of all complexes increased the T_m. The nickel and copper complexes (figure 5) show hypochromicity with increased T_m of 65 ± 1°C ($\Delta T_m = 7$°C) and 62 ± 1°C ($\Delta T_m = 4$°C), respectively, which is characteristic of intercalative binding [27]. All other compounds show little variation in T_m with $\Delta T_m = 2$–3°C, in turn supporting the observations made in the absorption and hydrodynamic experiments.
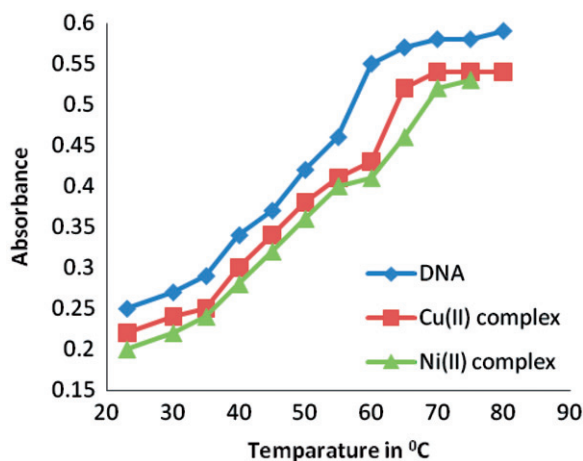
Figure 5. Effect of added complexes on the melting temperature (T_m) of *E. coli* DNA.

3.2.2.4. *Gel electrophoresis method.* Suitably designed metal complexes can induce several changes in DNA conformation after the complex has been bound. Metal complexes, which could induce DNA deformations, such as bending, "local denaturation" (overwinding and underwinding), intercalation, microloop formation, and subsequent DNA shortening, lead to decrease in molecular weight of DNA. Gel electrophoresis is an extensively used technique for study of binding of compounds with nucleic acids. In this method, segregation of the molecules will be on the basis of their relative rate of movement through a gel under the influence of an electric field. DNA is negatively charged and when placed in an electric field, it migrates toward the anode. The extent of migration of DNA depends on the strength of electric field, buffer, density of agarose gel, and size of the DNA. Generally, mobility of DNA is inversely proportional to its size. (Gel electrophoresis is shown in figure S2, Supplementary material.) The photograph shows bands with different bandwidth and brightness compared to the control. The difference observed in the intensity and the band width is the criterion for evaluation of binding ability of ligand and its transition metal complexes with DNA of *E. coli*. Lane C representing control experiment, where unaided DNA is used, does not show any significant cleavage of DNA even after longer exposure time. The intensity and mobility (tailing) of lanes I and II are same as the control band, indicating that there is no significant binding/cleavage of DNA by ligand and Co[II] complex. In lanes IV and V, width of the DNA band is enlarged due to the tailing and shows little increase in intensity, which may be attributed to binding of Cu[II] and Zn[II] complexes to DNA to a small extent. In lane III, the high intensity band with maximum tailing suggests strong binding of Ni[II] complex to DNA. The results suggest that binding of metal complexes caused a change in the conformation of DNA from intercalation and thus an increase in intensity of the band [28].

4. Conclusion

The ligand is a hexadentate monobasic chelate with N_4S_2 donating sites. The electrochemically active copper complex has binuclear structure with ligand to metal

ratio $2:2$ with octahedral geometry around each copper and is a $1:2$ electrolyte. The Co^{II}, Ni^{II}, and Zn^{II} complexes are octahedral with ligand to metal ratio $1:2$. Being a derivative of pyrazole, the ligand possesses significant activity against microbes which is further enhanced upon complexation. The DNA-binding studies reveal classical intercalation of the compounds. The Ni^{II} and Cu^{II} complexes exhibit higher binding ability than the rest.

This study reveals that the antimicrobial activity exhibited by the compounds can be correlated with their DNA binding ability. Compounds binding through intercalative mode to DNA prevent further replication, leading to death of the cell; the same mechanism is anticipated for anticancer activity of the compounds. Further structural modifications are presently being investigated to improve the potency as well as selectivity which may lead to potential anticancer agents.

In our laboratory, we have prepared similar ligand systems with different, substituted thiosemicarbazide arms. Analysis of the antimicrobial and DNA binding properties of complexes derived from these ligands is under progress.

Acknowledgments

References

[1] V.K. Tandon, D.B. Yadav, A.K. Chaturvedi, P.K. Shukla. *Bioorg. Med. Chem. Lett.*, **15**, 3288 (2005).
[2] D.K. Sau, R.J. Butcher, S. Chaudhuri, N. Saha. *Mol. Cell. Biochem.*, **253**, 21 (2003).
[3] M. Munakata, L.P. Wu, M. Yamamoto, T. Kuroda-Sowa, M. Maekawa, S. Kawata, S. Kitagawa. *J. Chem. Soc., Dalton Trans.*, 4099 (1995).
[4] T.C. Schenck, J.M. Dowens, C.R.C. Milne, P.B. Mackenzie, H. Boucher, J. Whelan, B. Bosnich. *Inorg. Chem.*, **24**, 2334 (1985).
[5] F. Meyer, A. Jacobi, B. Nuber, P. Rutsch, L. Zsolnai. *Inorg. Chem.*, **37**, 1213 (1998).
[6] S. Budagumpi, G.S. Kurdekar, G.S. Hegde, N.H. Bevinahalli, V.K. Revankar. *J. Coord. Chem.*, **63**, 1430 (2010).
[7] A. Silvestri, G. Barone, G. Ruisi, M. Teresa, L. Giudice, T. Salvatore. *J. Inorg. Biochem.*, **98**, 589 (2004).
[8] N. Raman, A. Saktivel, R. Jeyamurugan. *J. Coord. Chem.*, **62**, 3969 (2009).
[9] K.A. Kumar, K.L. Reddy, S. Satyanarayana. *J. Coord. Chem.*, **63**, 3676 (2010).
[10] X.W. Zhang, Y.J. Zhenga, Y.T. Lia, Z.Y. Wua, C.W. Yan. *J. Coord. Chem.*, **63**, 2985 (2010).
[11] K.L. Reddy, K.A. Kumar, S. Vidhish, P.N. Babu, S. Satyanarayana. *J. Coord. Chem.*, **62**, 3997 (2009).
[12] X.W. Lia, M. Jiang, Y.T. Li, Z.Y. Wua, C.W. Yan. *J. Coord. Chem.*, **63**, 1582 (2010).
[13] A.I. Vogel. *A Text book of Quantitative Inorganic Analysis*, 3rd Edn, Longmans Green and Co. Ltd., London (1961).
[14] N. Li, Y. Ma, C. Yang, L. Guo, X. Yang. *Biophys. Chem.*, **116**, 199 (2005).
[15] A. Arslantas, A.K. Devrim, H. Necefoglu. *Int. J. Mol. Sci.*, **8**, 564 (2007).
[16] W.J. Geary. *Coord. Chem. Rev.*, **7**, 81 (1971).
[17] A.D. Naik, S.M. Annigeri, U.B. Gnagadharmath, V.K. Revankar, V.B. Mahale, V.K. Reddy. *Indian J. Chem.*, **41A**, 2046 (2002).
[18] S. Budagumpi, M.P. Sathisha, N.V. Kulkarni, G.S. Kurdekar, V.K. Revankar. *J. Incl. Phenom. Macrocycl. Chem.*, **66**, 327 (2010).

[19] N.V. Kulkarni, G.S. Hegde, G.S. Kurdekar, S. Budagumpi, M.P. Sathisha, V.K. Revankar. *Spectrosc. Lett.*, **43**, 235 (2010).
[20] J. Pons, X. Lopez, E. Benet, J. Casabo, F. Teixidor, F.J. Sanchez. *Polyhedron*, **9**, 2839 (1990).
[21] A.B.P. Lever. *Inorganic Electronic Spectroscopy*, Elsevier Publishing Company, New York (1968).
[22] J.C. Bailar, H.J. Emeleus, R. Nyholm, A.F.T. Dickenson. *Comprehensive Inorganic Chemistry*, p. 3, Pergamon Press, Oxford (1975).
[23] R.L. Dutta, A. Syamal. *Elements of Magnetochemistry*, 2nd Edn, E W Press, New Delhi (1993).
[24] C.L. Bailey, R.D. Bereman, D.P. Rillema. *Inorg. Chem.*, **25**, 3149 (1986).
[25] A.M. Pyle, J.P. Rehmann, R. Meshoyrer, C.V. Kumar, N.J. Turro, J.K. Barton. *J. Am. Chem. Soc.*, **111**, 3051 (1989).
[26] S. Satyanarayana, J.C. Dabrowiak, J.B. Chaires. *Biochemistry*, **31**, 9319 (1992).
[27] S. Arounaguiri, B.G. Maiya. *Inorg. Chem.*, **35**, 4267 (1996).
[28] A. Arslantas, A.K. Devrim, N. Kaya, N. Necefoglu. *Int. J. Mol. Sci.*, **7**, 111 (2006).